Received: 15 April 2023 | Revised: 14 June 2023 | Accepted: 17 June 2023

DOI: 10.1002/mp.16631

RESEARCH ARTICLE

MEDICAL PHYSICS

MR-guided ion therapy: Detector response in magnetic fields during carbon ion irradiation

Hermann Fuchs[1,2] | **Fatima Padilla-Cabal**[1] | **Dietmar Georg**[1,2] | **Hugo Palmans**[2,3]

[1]Division of Medical Radiation Physics, Department of Radiation Oncology, Medical University of Vienna, Vienna, Austria

[2]MedAustron Ion Therapy Center, Wiener Neustadt, Wiener Neustadt, Austria

[3]National Physical Laboratory, Teddington, UK

Correspondence
Hermann Fuchs, Division of Medical Radiation Physics, Department of Radiation Oncology, Medical University of Vienna, Vienna, Austria.
Email: hermann.fuchs@meduniwien.ac.at

Abstract

Background: Combining carbon ion therapy with on-bed MR imaging has the potential to bring particle therapy to a new level of precision. However, the introduction of magnetic fields brings challenges for dosimetry and quality assurance. For protons, a small, but significant change in detector response was shown in the presence of magnetic fields previously. For carbon ion beams, so far no such experiments have been performed.

Purpose: To investigate the influence of external magnetic fields on the response of air-filled ionization chambers.

Methods: Four commercially available ionization chambers, three thimble type (Farmer, Semiflex, and PinPoint), and a plane parallel (Bragg peak) detector were investigated. Detectors were aligned in water such that their effective point of measurement was located at 2 cm depth. Irradiations were performed using 10×10 cm^2 square fields for carbon ions of 186.1, 272.5, and 402.8 MeV/u employing magnetic field strengths of 0, 0.25, 0.5, and 1 T. In addition, the detector response for protons and carbon ions was compared taking into account the secondary electron spectra and employing protons of 252.7 MeV for comparison.

Results: For all four detectors, a statistically significant change in detector response, dependent on the magnetic field strength, was found. The effect was more pronounced for higher energies. The highest effects were found at 0.5 T for the PinPoint detector with a change in detector response of 1.1%. The response of different detector types appeared to be related to the cavity diameter. For proton and carbon ion irradiation with similar secondary electron spectra, the change in detector response was larger for carbon ions compared to protons.

Conclusion:A small, but significant dependence of the detector response was found for carbon ion irradiation in a magnetic field. The effect was found to be larger for smaller cavity diameters and at medium magnetic field strengths. Changes in detector response were more pronounced for carbon ions compared to protons.

KEYWORDS
magnetic fields, MR-guided ion therapy, MR-guided proton therapy

1 | INTRODUCTION

The combination of on-bed MR imaging, coupled with radiation therapy was already introduced into clinical routine with the hybrid MR-linacs.[1–3] The superior soft-tissue contrast in combination with zero imaging dose coupled with on-bed imaging allows new treatment possibilities. For MR-linacs, it was already shown that a potential reduction of treatment margins can lead to a lower total irradiated volume.[4]

Ion-beam therapy, using protons or carbon ions for treatment, with its improved physical characteristics allows a more conformal dose distribution compared to conventional photon therapy. On-line imaging for precise anatomy, target, and organ-at-risk location, may be even more effective for ion-beam therapy, further increasing the treatment conformity and efficacy.[5] In addition, on-line surveillance of the target and the resulting improved positional accuracy could allow the introduction of new concepts, such as LET painting.

For ion-beam therapy, the primary treatment beam itself is influenced by the magnetic fields of such an hybrid MR system leading to dose perturbations, which need to be compensated.[5–10] The combination of MR imaging with carbon ion irradiation, MR-guided ion therapy (MRgIT), is still in its infancy. However, the further improved biological efficacy over protons makes it an obvious candidate besides MR-guided proton therapy.

The possibility to perform accurate dosimetry within magnetic fields is a key precondition for future clinical application of MRgIT. For MR-linacs, a considerable influence of magnetic fields of up to and beyond 10% on the detector response was shown.[11] Due to the different processes, these results can not be directly related to particle therapy. For proton irradiation in magnetic fields, changes in detector response between −0.7 and 0.5% depending on the detector type and magnetic field strength were observed.[12] The effects were small, but for absolute dosimetry and beam calibration should be accounted for.

So far, no experimental or in silico investigations of ionization chamber response have been performed for carbon ions in the presence of magnetic fields. The impact of an external magnetic field on the detector response is likely dependent on the secondary electron spectra, responsible for the magnitude of the signal generated in ionization chambers. For carbon ions, secondary electrons have higher energies compared to protons of comparable range in water,[13,14] consequently different correction factors are expected.

In this manuscript, we investigate four commercially available ionization chambers, one plane-parallel and three thimble type detectors, for magnetic field strengths of up to 1 T. Detectors were selected to cover a wide range of chamber diameters and active volumes.

Furthermore, the detector response for proton and carbon ions is investigated based on the secondary electron spectra of the respective particles.

2 | MATERIALS AND METHODS

2.1 | Set-up

A detailed description of the magnet and measurement set-up can be found elsewhere,[12,15] in the following only a short overview is given. A resistive dipole magnet (Danfysik A/S, Taastrup, Denmark) with a pole gap of 13.5 cm and a pole diameter of 25 cm was placed in front of the horizontal research beam line at the MedAustron ion therapy center (Wr. Neustadt, Austria). The magnet is capable of producing magnetic field strengths up to 1 T. Positioning was such that the magnetic field center coincided with the room isocenter (see Figure 1). A detailed characterization of the beam line, the magnetic fields and the corresponding beam path deviations due to the Lorentz force were performed earlier.[15] The beam line is equipped with a clinical nozzle and allows spot scanning with a maximum field size of 20×20 cm^2 over the clinical energy range from 62.4 to 252.7 MeV and 120.0 to 402.8 MeV/u for protons and carbon ion beams, respectively.

A custom-designed motorized water phantom[12] with outer dimensions of $8 \times 40 \times 15$ cm^3 was employed for detector positioning. The phantom surface was located 12.5 cm proximal to the isocenter. Detector positioning at a water-equivalent depth of 2 cm was facilitated by the use of the TruFix system (PTW, Freiburg, Germany), employing in-house designed adapters to fix the TruFix system in the water phantom. This positioning, taking into account the entrance window cut-out, placed the EPOM 9.5 cm proximal to the isocenter.

The TruFix system is machined such that detectors are positioned according to their EPOM as defined in DIN-6800-2.[16] For plane parallel detectors, this is the inner side of the entrance window, for cylindrical detectors, a shift of $0.5 \times r_{cyl}$ from the cavity center z_{ref}. For heavy ions, TRS-398 recommends a value of $0.75 \times r_{cyl}$ for cylindrical detectors, a correction which was not performed due to the minute changes. An overview of the used positions and the deviations towards the TRS-398 recommendation for heavy ions can be found in Table 1. TRS-398 recommends to measure in the spread-out Bragg peak.[17] However, at MedAustron, reference dose measurements are performed at shallow depth, as it was shown that the same formalism can be used.[18]

The detector EPOM is located at the beginning of the homogeneous region of the magnetic field, reducing the primary beam deflection at the point of measurement. To reduce beam time, measurements with two thimble type detectors were performed simultaneously, with a vertical distance of 25 mm between the effective points of measurement (see Figure 1).

2.2 | Investigated detectors

Three thimble type (Farmer, PinPoint, and Semiflex) and one plane-parallel (small diameter Bragg peak) ionization chambers (PTW, Freiburg, Germany) were selected, covering a wide range of active volumes. The detector volumes of the selected thimble type detectors cover a wide range of available active volumes (0.6–0.016 cm^3). An overview of the employed detectors including their reference point can be found in Table 1. Detectors were connected to Unidos Webline electrom-

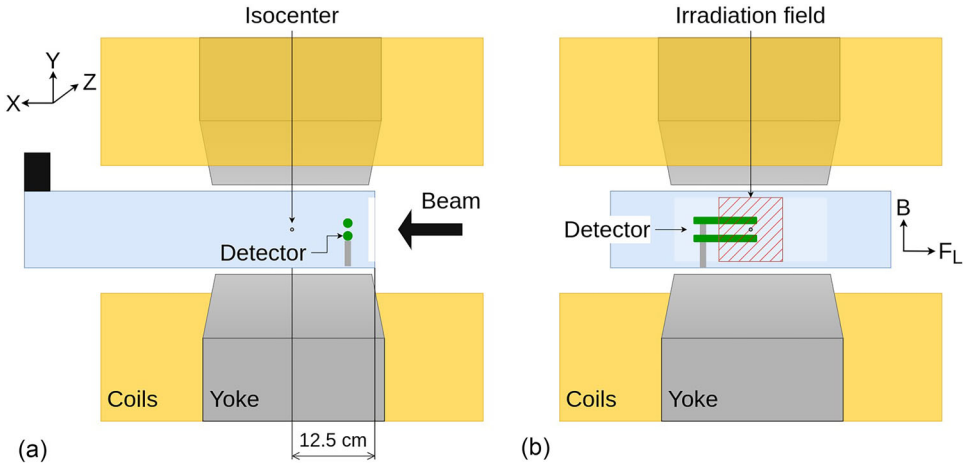

FIGURE 1 Sketch of the experimental set-up within the research dipole magnet positioned at the isocentre. The beam is impinging on the water phantom located between the magnet poles from the right hand side. Light-orange rectangles mark the position of the magnet coils, the magnet yokes are colored in dark gray, the water phantom in light blue, and the detectors in green.

TABLE 1 Investigated detectors, active volume, cavity diameter (for the plane parallel detector, the cavity thickness is presented), the effective position of the ionization chamber's reference point, P_{eff}, as well as the offset of the EPOM between the DIN 6800-2 as used by the TruFix system (PTW, Freiburg, Germany) and the recommendations for heavy ions according to TRS-398 recommendations.

Detector	Type	Active volume [cm^3]	Cavity diameter [mm]	z_{ref} [cm]	Δz_{ref} to TRS-398 [cm]
PTW-34073	Small diameter Bragg peak-type PPIC	2.5	2.0	2.00	0.00
PTW-30013	Farmer-type thimble IC	0.6	6.1	2.15	0.08
PTW-31013	Semiflex-type thimble IC	0.3	5.5	2.14	0.07
PTW-31016	PinPoint-type thimble IC	0.016	2.9	2.07	0.04

eters (PTW, Freiburg, Germany). The detectors used in this study were not certified to be magnetic field compatible. However, functional tests performed before and after the exposure to magnetic fields showed no adverse effects on the detector performance.

2.3 | Measurements

After detector alignment within the water phantom and the dipole magnet, every detector was pre-irradiated with a physical dose of 15 Gy. After pre-irradiation, a charge leakage correction (e.g., a zeroing of the electrometer) was performed.

Irradiations used square fields of 10×10 cm^2 of single-energy particles employing a 2 mm spot spacing in both horizontal and vertical direction with constant spot weighting. Measurements were performed for one nominal proton energy (252.7 MeV) and up to three nominal carbon ion energies (186.1, 272.5, and 402.8 MeV/u) for magnetic fields of 0, 0.25, 0.5, and 1 T. The magnetic field value at the center of the magnet was verified using a single-axis hall probe AS-NTM connected to a FM 302 Teslameter (Projekt Elektronik Mess- und Regelungstechnik GmbH, Berlin, Germany). Deviations between nominal and measured values were found to be within 3 mT.

TABLE 2 c_B factors for the Bragg peak detector, calculated as the ration of dose to water at the point of measurement with and without an applied magnetic field of 1 T, based on Monte Carlo simulations.

Detector	Particle	Energy [MeV/u]	c_B
BP	P	252.7	1.0004
	C12	186.1	0.9984
	C12	272.5	0.9998
	C12	402.8	0.9994

All four detectors were investigated using carbon ion beams at 402.8 MeV/u. In addition, to investigate a potential energy dependence, for the Bragg peak detector, three carbon ion energies (186.1, 272.5, and 402.8 MeV/u) were investigated, corresponding to ranges in water from 70 to 280 mm.

For all detectors and energies, measurements were performed in the same set-up, without repositioning. Magnetic field strengths were applied in sequential cycles. Typically five measurements were acquired per energy, and field strength before changing the magnetic field. After each magnetic field, measurements at 0 T

TABLE 3 Summary of measured data for the three thimble type detectors for carbon ion beams.

Detector	Energy [MeV/u]	B [T]	#Meas	$k_{B,M,Q}$	STDev [%]	STDOM [%]	Mann–Whitney-*U* test *P*-value
Farmer	402.8	0	36	1.000	0.22	0.04	
		0.25	28	1.005	0.26	0.05	<0.001*
		0.5	28	1.003	0.29	0.05	<0.001*
		1	28	1.000	0.27	0.05	0.951
	272.5	0	35	1.000	0.21	0.03	
		0.25	20	1.004	0.27	0.06	<0.001*
		0.5	20	1.002	0.27	0.06	0.004*
		1	20	0.999	0.32	0.07	0.479
Semiflex	402.8	0	35	1.000	0.16	0.03	
		0.25	28	1.005	0.23	0.04	<0.001*
		0.5	28	1.004	0.25	0.05	<.001*
		1	28	1.001	0.21	0.04	0.265
PinPoint	272.5	0	35	1.000	0.45	0.08	
		0.25	19	1.009	0.50	0.12	<0.001*
		0.5	20	1.011	0.54	0.12	<0.001*
		1	20	1.009	0.59	0.13	<0.001*
		402.8	35	1.000	0.16	0.03	
		0.25	20	1.009	0.23	0.04	<0.001*
		0.5	21	1.010	0.25	0.05	<0.001*
		1	25	1.009	0.21	0.04	<0.001*

Note: A * highlights statistically significant deviations.

TABLE 4 Summary of measured data for the Bragg peak detectors for carbon ion beams.

Detector	Energy [MeV/u]	B [T]	#Meas	$k_{B,M,Q}$	STDev [%]	STDOM [%]		Mann–Whitney-*U* test *P*-value
Bragg peak	402.8	0	51	1.000	0.12		0.02	
		0.25	25	1.008	0.14	0.03		<0.001*
		0.5	25	1.009	0.16	0.03		<0.001*
		1	25	1.004	0.15	0.03		<0.001*
	272.5	0	35	1.000	0.10		0.02	
		0.25	20	1.007	0.11	0.03		<0.001*
		0.5	20	1.007	0.12	0.03		<0.001*
		1	20	1.000	0.11	0.03		0.472
	186.1	0	32	1.000	0.09		0.02	
		0.25	19	1.004	0.13	0.03		<0.001*
		0.5	19	1.004	0.13	0.03		<0.001*
		1	19	0.998	0.11	0.03		<0.001*

Note: A * highlights statistically significant deviations.

were interposed. This cycle was repeated several times. In total, this resulted in 19–53 measurements acquired per energy, detector, and magnetic field strength (a detailed overview of the acquired number of measurements can be found in Tables 3 and 4). Protons and carbon ion beams were measured at different days.

Dose levels were chosen to achieve comparable measurement uncertainties for protons and carbon ion beams, resulting in physical doses of 0.2 and 2.4 Gy for protons and carbon ion beams, respectively. The initially investigated 0.2 Gy dose level for carbon ion beams, exhibited too high variances because of limitations of our beam delivery system with low number of particles

per spot. For the selected detector position, particles, and energies, lateral beam displacement at the point of measurement due to the magnetic field was evaluated with Monte Carlo simulations to be 5 mm for protons, and 2–3 mm for carbon ion beams.[15] Consequently, the irradiation field was not shifted to re-center the detectors in the center of the irradiation field, keeping the delivered irradiation plans constant for all magnetic field strengths.

2.4 | Dose constancy in the presence of magnetic fields

Our approach assumed that the dose to water at the point of measurement is not affected by the applied magnetic field. For photons, this is typically not the case.[11] For charged particles, a small change in the particle range was observed earlier.[15] A more prominent contribution may be expected due to the lateral displacement of the irradiation field due to the Lorentz force. To investigate a potential change of the dose to water at the point of measurement, Monte Carlo simulations were performed using our commissioned Monte Carlo tool GATE.[15] A cylindrical geometry mimicking the active volume of the largest detector, the Bragg peak detector, was placed in water at the measurement position z_{ref}. Within this volume, the dose to water was scored with and without an applied magnetic field of 1 T. Statistical uncertainty was kept below 0.1%. Using this data, a correction factor c_B was calculated,[11,19]

$$c_B = \frac{\frac{D^B_{w,Q_{msr}}}{\phi^B}}{\frac{D_{w,Q_{msr}}}{\phi}} \tag{1}$$

where $D^B_{w,Q_{msr}}$ and $D_{w,Q_{msr}}$ are the dose to water with the given radiation quality Q_{msr} with and without a magnetic field B, respectively, for a given fluence ϕ^B with and without magnetic field B.

2.5 | Electron spectra

A considerable contribution to the signal generated in an ionization chamber is caused by secondary electrons with kinetic energies that allow them to traverse the ionization chamber geometry. To investigate whether magnetic field correction factors are dependent on the primary ion type, measurements at irradiation energies with similar secondary energy spectra at the point of measurement were performed. A suitable carbon ion energy with an electron spectrum similar to the highest proton energy available (252.7 MeV) was identified using Monte Carlo simulations. GATE version 9.2 based upon Geant4.11.00p01 was used for simulations, employing the MedAustron research room beam model.[20,21] The experimental set-up without magnetic fields was recreated, scoring the electron spectra at a water-equivalent depth of 2 cm. Multiple carbon ion energies were tested. In Geant4 cutoffs are specified in terms of range in the respective material. A production cutoff of 1 μm for secondary particles was used, corresponding to an energy cutoff well below 10 keV for electrons in water.

The electron spectrum of a carbon ion energy of 272.5 MeV/u was found to match the proton electron spectra of 252.7 MeV closely (see Figure 2). Consequently, the Bragg peak, Farmer, as well as the PinPoint detector were also investigated at 252.7 MeV protons and 272.5 MeV/u carbon ion beams.

At these energies, carbon ions created about 33 times more electrons of an energy above the cutoff compared to protons, whereas the total stopping power was about 36 times higher.

2.6 | Data analysis

Absorbed dose values in water with an ionization chamber were determined according to TRS-398 (Equation 2)

$$D_{w,Q} = M_Q N_{D,w,Q_0} k_{Q,Q_0} \tag{2}$$

where Q is the reference beam quality, Q_0 is the calibration beam quality, N_{D,w,Q_0} the calibration coefficient in terms of absorbed dose to water, and k_{Q,Q_0} the beam quality correction factor. We followed the procedure described in Fuchs et al.[12] and defined a magnetic field correction factor $k_{B,M,Q}$ accounting for the change of detector response due to an applied magnetic field (Equation 3):

$$k_{B,M,Q} = \frac{M_Q}{M^B_Q} \tag{3}$$

where M^B_Q is the detector reading with and M_Q to the detector reading without applied magnetic field B. This evaluation was performed with M^B_Q, and M_Q after performing temperature and pressure correction according to TRS-398.[17] No further corrections were applied.

Data analysis was performed using Python 3.9.15 employing numpy, pandas, scipy and the statistics package. The normality of the distribution of the measurement data was evaluated using a Shapiro–Wilk test. For the Bragg peak detector, a small drift, similar as reported for protons,[12] was observed during the measurements. This drift was found to be small, not requiring a correction. However, it resulted in a non-Gaussian distribution, rendering the Student's *t*-test not applicable. For consistency, we evaluated all data employing

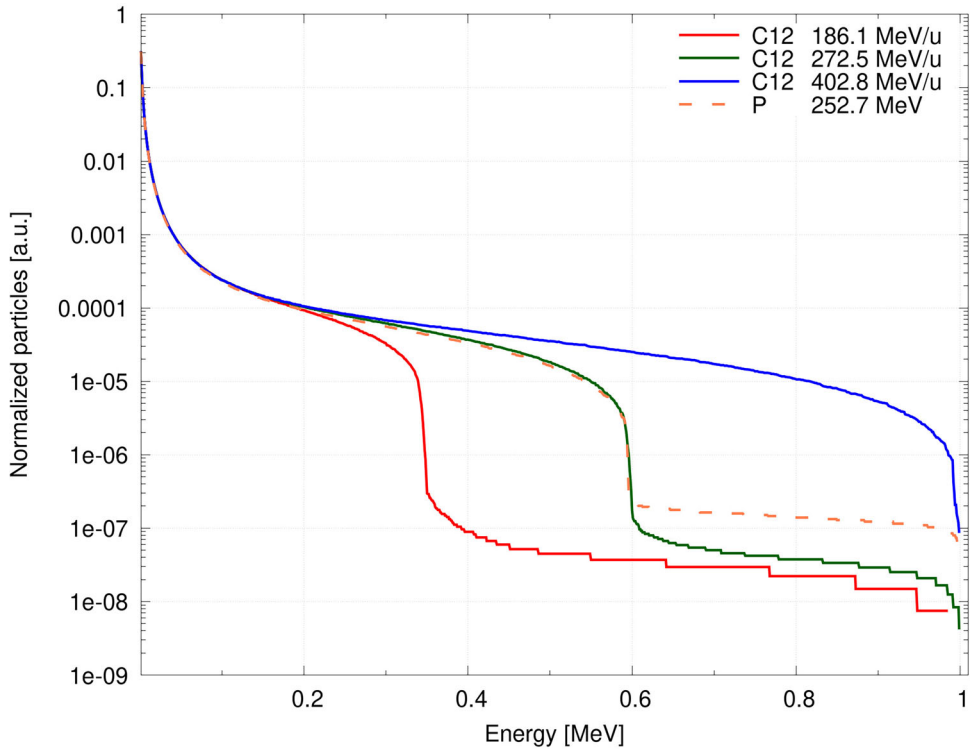

FIGURE 2 Electron spectra simulated using GATE 9.2 in water, scored at a water equivalent depth of 2 cm. Simulated for 252.7 MeV protons (black dashed line), and 186.1 , 272.5 , and 402.8 MeV/u carbon ion beams (solid red, green, and blue lines, respectively).

the two-sided Mann–Whitney-*U* test with a significance level of $P < 0.05$. The standard deviation of the means (STDOM) was calculated and used to describe the type-A measurement uncertainty.

3 | RESULTS

A summary of the measurement data for all four ionization chambers can be found in Tables 3 and 4, with a visualization of the measured data displayed in Figure 3.

3.1 | Magnetic field dependence

In a first step, the magnetic field correction factor $k_{B,M,Q}$ was investigated at the highest carbon ion energy (402.8 MeV/u) (see Figure 4). All investigated detectors exhibited a change of chamber response dependent on the magnetic field. Most $k_{B,M,Q}$ factors were found to be highly statistically significantly different from unity, with *P*-values below 0.001. For the Farmer and the Semiflex detector, $k_{B,M,Q}$ at 1 T was found not to be distinguishable from the value at 0 T.

$k_{B,M,Q}$ increased with increasing field strength, reached a maximum and then reduced at higher field strengths, for some detectors returning to unity. The effect appeared to be correlated with the diameter of the active volume in beam direction, with higher effects for the smallest diameter (see Table 1). The highest deviation of 1.1% compared to the response at 0 T was found for the PinPoint detector at 0.5 T.

3.2 | Energy dependence

Overall, $k_{B,M,Q}$ was shown to increase with increasing carbon ion energy, although the detector behavior was similar for all energies (see Figure 5). For the Bragg peak detector, the highest deviation from 0 T was found with 0.9% for 402.8 MeV/u at 0.5 T.

3.3 | Dose constancy at the measurement position

The c_B factor for the Bragg peak detector geometry, the used particles and energies, calculated from Monte Carlo simulations can be found in Table 2 with the largest difference to unity of 0.9984 for carbon ions of 186.1 MeV/u.

3.4 | Comparison to protons

Overall, the behavior of the detectors was found to be similar for protons and carbon ion beams (see Figure 6). The effect was larger for carbon ion beams and more

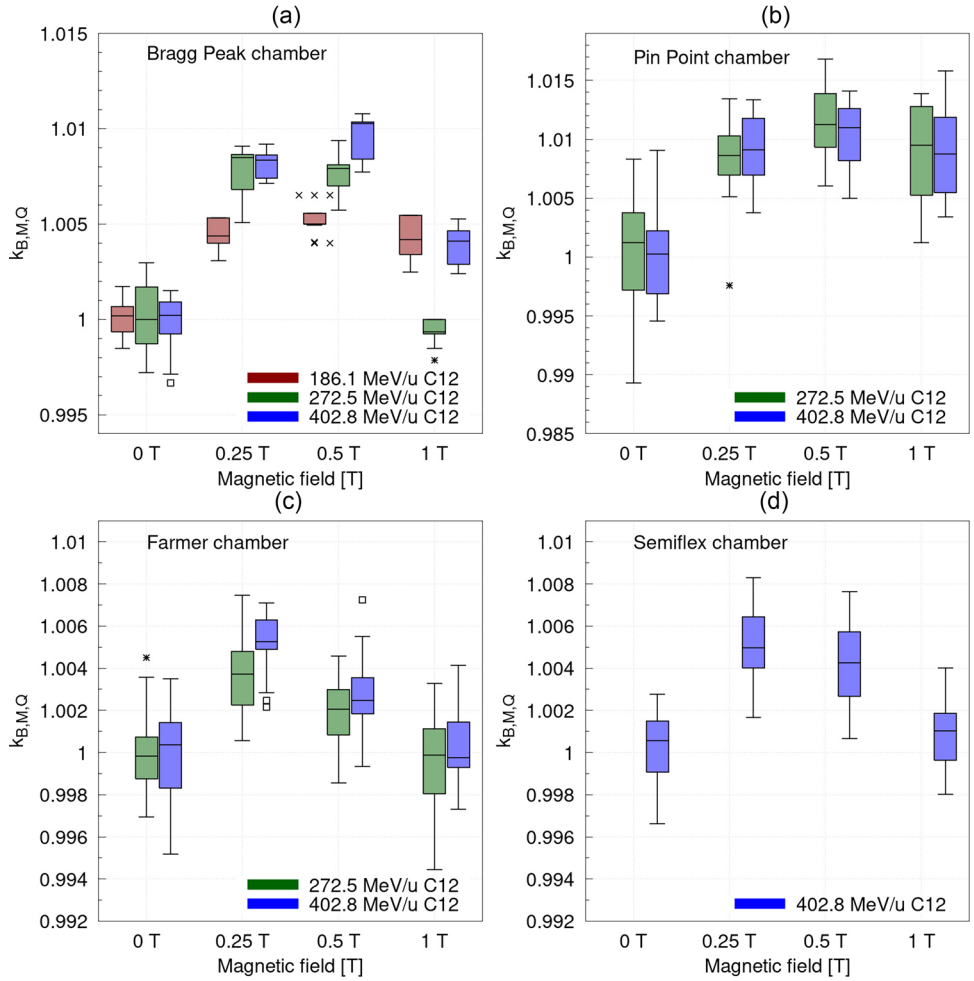

FIGURE 3 Magnetic field correction factor $k_{B,M,Q}$ for the (a) small diameter Bragg peak (act. volume 2.5 cm^3), (b) PinPoint (act. volume 0.016 cm^3), (c) Farmer (act. volume 0.6 cm^3), and (d) Semiflex (act. volume 0.3 cm^3) chamber for all measured carbon ion energies and all four magnetic field strengths (0, 0.25, 0.5, and 1 T). The shaded area indicates the standard deviation of the means (STDOM).

pronounced for smaller detector diameters. Carbon ion correction factors $k_{B,M,Q}$ were found to be consistently higher compared to protons.

4 | DISCUSSION

The chosen point of measurement was found to be at the edge of the homogeneous magnetic field. Repeated modeling calculations showed a deviation of the magnetic field strength at the EPOM of less than 3%. We kept the measurement position to allow an easy comparison to the previous publication as well as to benefit from the low changes in beam trajectories.

The change in detector response between different detectors, appears to be influenced by the cavity dimension in the beam direction and only indirectly by the active volume itself. This was supported by the relatively minor difference between the Farmer and Semiflex detector, exhibiting a factor of two difference in active detector volume, but similar cavity diameters (see Figure 4 and Table 1).

Only a very minute difference of the dose to water at the point of measurements with and without an applied magnetic field was found. We believe that this can be attributed to two factors. First, the irradiation field was not compensated for the lateral displacement due to the magnetic field. However, maximum displacements were found to be 5 mm for protons which, given the field size of 10×10 cm^2, should be negligible. We decided to keep the same irradiation field to enable easier comparison with previous measurements.[12] Second, a reduction of the range in the initial beam direction owing to the bending of the beam trajectory due to the magnetic field. For protons of 252.5 MeV, the total range reduction of 2 mm was larger than for carbon ion beams. In our case, the measurements were performed at approximately 5% of the total range, consequently only a submillimetric shift due to the range reduction should be present at the measurement position. The results indicate that lateral

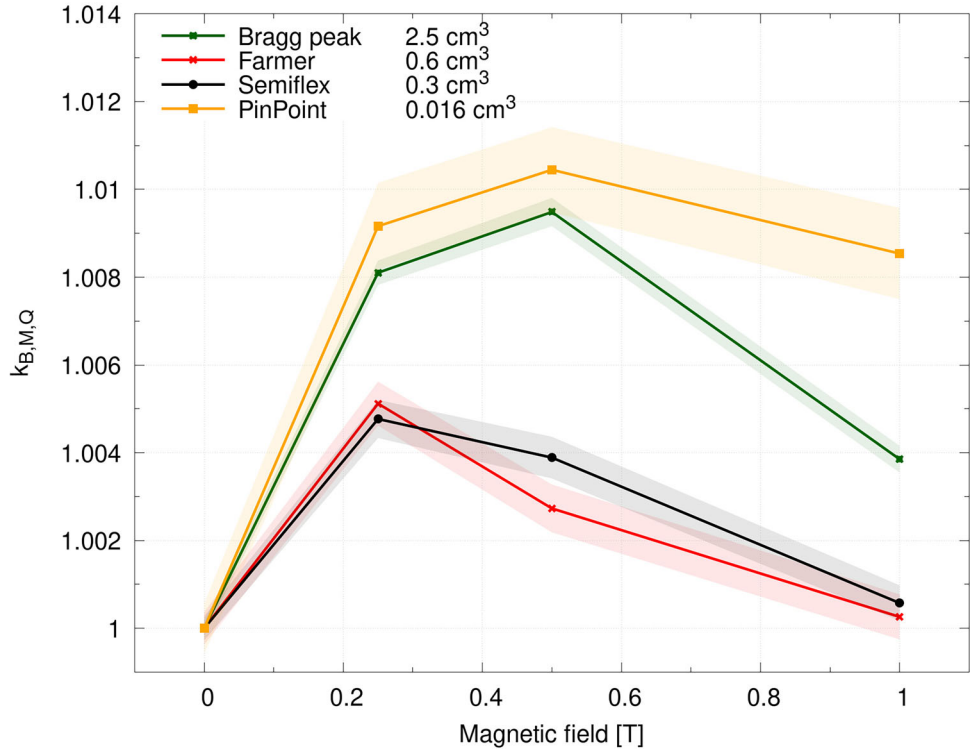

FIGURE 4 Magnetic field correction factor $k_{B,M,Q}$ for four commercial ionization chambers (small diameter Bragg Peak (act. volume 2.5 cm^3), PinPoint (act. volume 0.016 cm^3), Farmer (act. volume 0.6 cm^3), and Semiflex (act. volume 0.3 cm^3)) using the highest carbon ion energy (402.8 MeV/u) and four magnetic field strengths (0, 0.25, 0.5, and 1 T). The shaded area indicates the standard uncertainty envelope based on the standard deviation of the means (STDOM) of the individual data points.

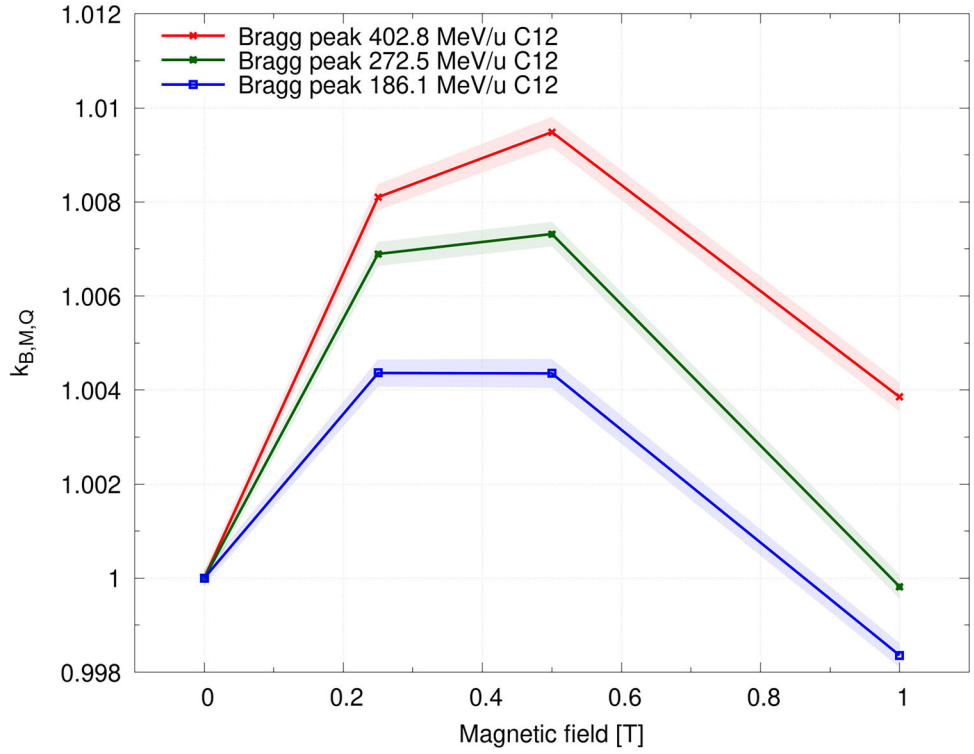

FIGURE 5 Relative detector response for the Bragg peak detector, measured with carbon ion beams of 186.1, 272.5, and 402.8 MeV/u for magnetic field strengths of 0, 0.25, 0.5, and 1 T. The shaded area indicates the standard deviation of the means (STDOM).

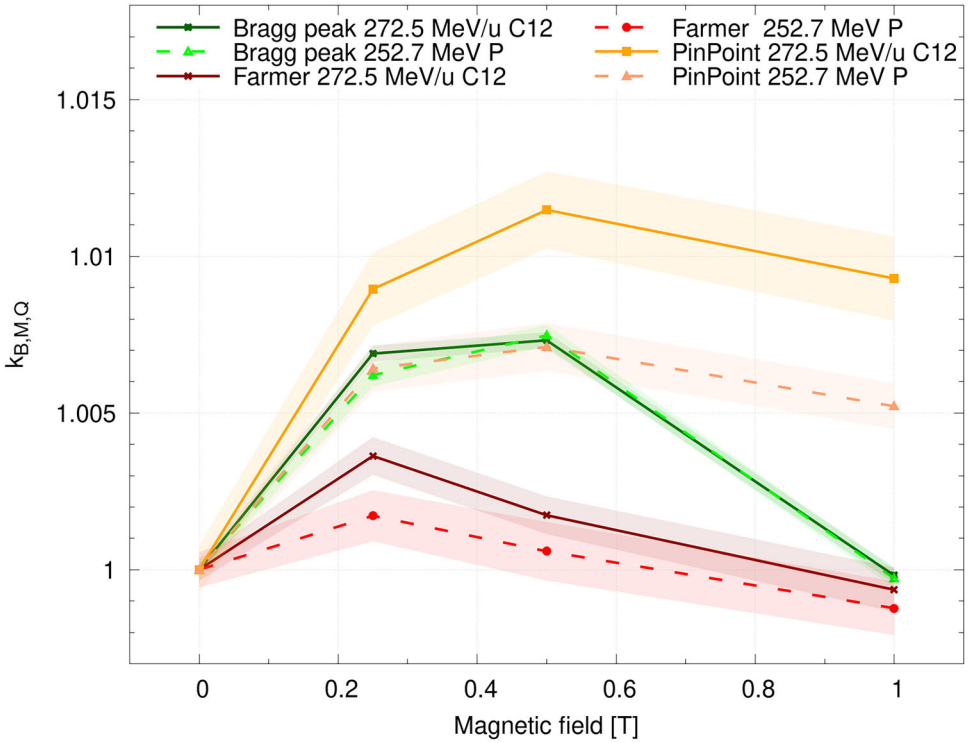

FIGURE 6 Relative detector response for the Bragg peak (act. volume 2.5 cm^3), Farmer (act. volume 0.6 cm^3), and PinPoint (act. volume 0.016 cm^3) detector for protons and carbon ion beams for magnetic field strengths of 0, 0.25, 0.5, and 1 T, measured at an energy with comparable secondary electron spectrum. Solid lines mark measurements using carbon ion beams, dashed lines for proton beams. The shaded area indicates the standard deviation of the means (STDOM).

displacements of the irradiation field due to the magnetic field of up to 5 mm, as well as the small changes in penetration depth, do not make a relevant contribution to the overall detector response change.

Our set-up enabled the irradiation at multiple magnetic field strengths for protons and carbon ion beams without repositioning, considerably reducing set-up uncertainties. For the Bragg peak detector, proton measurements performed earlier[12] were repeated, resulting in very similar $k_{B,M,Q}$ values as reported earlier with deviations of less than −0.1% for all magnetic field strengths.

Overall, the behavior of the detector response for protons and carbon ion beams was found to be similar, with a considerably larger effect for carbon ion beams. Similar to protons, besides a dependency on the magnetic field strength, a dependency on the primary beam energy was observed. The effect was found to be more pronounced for higher energies.

It was expected that the differences in detector response in magnetic fields due to the particle type were caused mainly by the different secondary electron spectra and maximum electron energies. Our initial hypotheses was that if an ideal match of the secondary electron spectra of protons and carbon ion could be achieved, both particle species should observe the same changes in $k_{B,M,Q}$ due to the presence of a magnetic field. A matching of the beam quality of the secondary electrons as close as possible was performed, trying to match the beam quality in the nanodosimetric sense. A matching in the presence of the magnetic field was not investigated. However, only submillimetric changes were observed in the remaining range and thus a close match can be expected.[8] Still, the carbon ion $k_{B,M,Q}$ was found to be higher compared to protons. A 9% difference between the dose and stopping power ratios was observed using Monte Carlo simulations, but it seemed unlikely that this accounted for the observed differences. To further investigate this, the restricted as well as the nonrestricted stopping power, following the formalism described in Paganetti et al.,[22] were evaluated for protons and carbon ion beams. A cutoff of 81 keV, as used for the electron spectra simulations above, was employed. The ratio of restricted versus nonrestricted stopping power for proton and carbon ion beams was almost identical with a ratio of 0.88. This indicates that the matching was as good as we could achieve it. The choice of the applied energy cutoff of 1μm was somewhat arbitrary, and chosen to evaluate also the low energy part of the secondary electron spectra.

The detailed reason for the difference in $k_{B,M,Q}$ between proton and carbon ions with closely matched secondary electron spectra remained unclear and needs to be investigated in more details, for example,

using Monte Carlo simulations, which include the effect of magnetic fields on particle transport and dosimetry.

5 | CONCLUSION

Four ionization chambers, three thimble type, and a plane parallel detector were investigated concerning their change in response due to the presence of magnetic fields, resulting in a small, but statistically significant change in detector response, dependent on the magnetic field strength, for all detectors. The effect is more pronounced for higher energies. Highest effects were found at 0.5 T for the PinPoint detector with a correction factor 1.1% different from unity. The cavity diameter in beam direction seems to be the dominant factor for detector response differences. For carbon ion irradiations with comparable energy spectra to protons, the change of chamber response was found to be higher.

ACKNOWLEDGMENTS

We would like to thank our colleagues from the MedAustron medical technicians and facility management team, especially Norbert Schmoll and Gernot Schönleitner, for their support and insightful discussions.

CONFLICT OF INTEREST STATEMENT

The authors declare no conflicts of interest.

REFERENCES

1. Raaymakers BW, Jürgenliemk-Schulz IM, Bol GH, et al. First patients treated with a 1.5T MRI-Linac: clinical proof of concept of a high-precision, high—first patients treated with a 1.5T MRI-Linac: clinical proof of concept of a high-precision, high-field MRI guided radiotherapy treatment. *Phys Med Biol*. 2017;62(23):L41-L50.
2. Nachbar M, Mönnich D, Boeke S, et al. Partial breast irradiation with the 1.5 T MR-Linac: first patient treatment and analysis of electron return and stream effects. *Radiother Oncol*. 2020;145:30-35.
3. Tijssen RH, Philippens ME, Paulson ES, et al. MRI commissioning of 1.5T MR-linac systems—a multi-institutional study. *Radiother Oncol*. 2019;132:114-120.
4. Spindeldreier CK, Klüter S, Hoegen P, et al. MR-guided radiotherapy of moving targets. *Radiologe*. 2021;61(S1):39-48.
5. Hoffmann A, Oborn B, Moteabbed M, et al. MR-guided proton therapy: a review and a preview. *Radiat Oncol*. 2020;15(1):129.
6. Padilla-Cabal F, Resch AF, Georg D, Fuchs H. Implementation of a dose calculation algorithm based on Monte Carlo simulations for treatment planning towards MRI guided ion beam therapy. *Physica Med*. 2020;74:155-165.
7. Padilla-Cabal F, Georg D, Fuchs H. A pencil beam algorithm for magnetic resonance image-guided proton therapy. *Med Phys*. 2018;45(5):2195-2204.
8. Fuchs H, Moser P, Gröschl M, Georg D. Magnetic field effects on particle beams and their implications for dose calculation in MR-guided particle therapy. *Med Phys*. 2017;44(3):1149-1156.
9. Schellhammer SM, Hoffmann AL, Gantz S, et al. Integrating a low-field open MR scanner with a static proton research beam line: proof of concept. *Phys Med Biol*. 2018;63(23):23LT01.
10. Schellhammer SM, Hoffmann AL. Prediction and compensation of magnetic beam deflection in MR-integrated proton therapy: a method optimized regarding accuracy, versatility and speed. *Phys Med Biol*. 2017;62(4):1548-1564.
11. de Pooter JA, Billas I, de Prez LA, et al. Reference dosimetry in MRI-linacs: evaluation of available protocols and data to establish a Code of Practice. *Phys Med Biol*. 2021;66(5):05TR02.
12. Fuchs H, Padilla-Cabal F, Zimmermann L, et al. MR-guided proton therapy: impact of magnetic fields on the detector response. *Med Phys*. 2021;48(5):2572-2579.
13. Scifoni E, Surdutovich E, Solov'yov AV. Spectra of secondary electrons generated in water by energetic ions. *Phys Rev E*. 2010;81(2):021903.
14. de Vera P, Abril I, Garcia-Molina R. Energy spectra of protons and generated secondary electrons around the Bragg peak in materials of interest in proton therapy. *Radiat Res*. 2018;190(3):282-297.
15. Fuchs H, Padilla-Cabal F, Oborn BM, Georg D. Commissioning a beam line for MR-guided particle therapy assisted by in silico methods. *Med Phys*. 2022. doi:10.1002/mp.16143
16. Zakaria A, Schuette W, Younan C. Reference dosimetry according to the new German protocol DIN 6800-2 and comparison with IAEA TRS 398 and AAPM TG 51. *Biomed Imaging Interv J*. 2011;7(2):e15.
17. Pedro A, Burns DT, Hohlfeld K, et al. *IAEA TRS 398: Absorbed Dose Determination in External Beam Radiotherapy: An International Code of Practice for Dosimetry based on Standards of Absorbed Dose to Water*. 2006.
18. Palmans H, Vatnitsky SM. Beam monitor calibration in scanned light-ion beams. *Med Phys*. 2016;43(11):5835-5847.
19. van Asselen B, Woodings SJ, Hackett SL, et al. A formalism for reference dosimetry in photon beams in the presence of a magnetic field. *Phys Med Biol*. 2018;63(12):125008.
20. Fuchs H, Elia A, Resch AF, et al. Computer-assisted beam modeling for particle therapy. *Med Phys*. 2021;48(2):841-851.
21. Elia A, Resch AF, Carlino A, et al. A GATE/Geant4 beam model for the MedAustron non-isocentric proton treatment plans quality assurance. *Physica Med*. 2020;71:115-123.
22. Palmans H. Detectors, relative dosimetry, and microdosimetry. In: Paganetti H, ed. *Proton Therapy Physics*. CRC Press; 2020:275-308.

How to cite this article: Fuchs H, Padilla-Cabal F, Georg D, Palmans H. MR-guided ion therapy: Detector response in magnetic fields during carbon ion irradiation. *Med Phys*. 2023;50:7167–7176. https://doi.org/10.1002/mp.16631